

**Project Title:**

**Computational Studies of Muon Locations, Electronic Structures and Electron Transport in High-Tc Superconductor, Organic, Organometallic and Biological Systems.**

**Name:**

○Shukri Sulaiman (1,2), Mohamed Ismail Mohamed-Ibrahim (1,2), Isao Watanabe (2), Harison Rozak (1,2), Fahmi Astuti (2,3), Muhammad Darwis Umar (2,3), Irwan Ramli (2,3), Julia Angel (2,3), Muhammad Redo Ramadhan (2,4), and Dita Puspita Sari (2,5).

**Laboratory at RIKEN:**

**Meson Science Laboratory**

(1) Universiti Sains Malaysia, Malaysia

(2) RIKEN, Nishina Center, Japan

(3) Hokkaido University, Japan

(4) Universitas Indonesia

(5) Shibaura Institute of Technology, Japan

1. Background and purpose of the project, relationship of the project with other projects

$\mu$ SR spectroscopic technique is an excellent nuclear method to study a wide range of problems in physics and chemistry. Various phenomena can be explored and understood such as hyperfine interactions, magnetism, and electron transport. This technique involves muon particles particularly the one with a positive charge. Here, muon serves as a dilute magnetic probe where spin-polarized  $S = \frac{1}{2}$  positive muons are implanted into a material.

In the  $\mu$ SR experiments, however, we are unable to determine the possible location of the muon, i.e. the exact place in the systems where the field is measured. Therefore, the theoretical calculations using First-Principles density functional theory (DFT) methods can be very valuable to obtain a general idea about the position of muon. The knowledge about the muon stopping sites would then enable a detailed comparison between microscopic theory and  $\mu$ SR data. This is crucial particularly for the analysis of magnetism, since the field experienced by the muon at that particular site, which characterized by the isotropic Fermi contact and anisotropic dipolar components

of the hyperfine coupling constant, is sensitive to the local magnetic ordering and the associated magnetic moment of the materials. A full picture of the electronic structures of the pure and muonated systems is the key to understanding the underlying physics behind the unique characteristics of each material and manipulating the parameters to synthesize new compounds with specific target properties.

In this project, our research group has focused on the studies of muon in six different host materials. The background study and characteristic interests of each target system are explained separately:

i. Organic magnets

There are two classes of organic molecular systems studied in this research,  $\beta^{\prime}X[\text{Pd}(\text{dmit})_2]_2$  [ $X = \text{EtMMe}_{4-n}(\text{P}, \text{Sb})$ ] and  $\kappa\text{-(BEDT-TTF)}_2\text{Cu}[\text{N}(\text{CN})_2]X$  ( $X = \text{Cl}, \text{Br}, \text{and D}$ ). These organic systems share some common characteristics, where both can be treated as two-dimensional systems and their physical properties are ultimately determined by the overlap of the molecular orbitals. They are also Mott insulators, which exhibit a variety

of physical properties including superconductivity under a certain pressure. However, the packing motif of the dimers in the two organic magnets is completely different. Despite the similar delocalized behavior of the unpaired electron in both classes of materials, the conducting part, where the unpaired spin resides in the materials, however, are different. In the case of  $\beta^{\pm}X[\text{Pd}(\text{dmit})_2]_2$ , the electron is distributed throughout the anion, whereas for  $\kappa\text{-(BEDT-TTF)}_2\text{Cu}[\text{N}(\text{CN})_2]X$  the electron is distributed throughout the cation. Additionally, the delocalization behavior of the unpaired electron in both organic magnets may lead to peculiar characteristics to the magnetic properties of the systems. Up to now, the magnetism of these materials remains unclear, particularly the magnetic structure of the systems. An appropriate quantum mechanical approach is employed to tackle these issues. The details on the background of these two kinds of materials are elaborated separately as below.

a)  $\beta^{\pm}X[\text{Pd}(\text{dmit})_2]_2$   $X=\text{EtnMe}_{4-n}(\text{P}, \text{Sb})$

$\beta^{\pm}X[\text{Pd}(\text{dmit})_2]_2$  where X is the cation, is an important class of ion radical salts that have many potential applications, especially in spintronics. The exploitation of their properties requires a thorough understanding of their electronic and magnetic properties at the microscopic level, particularly the magnetic ground state and the structure of their long-range magnetic ordering.

Several experimental investigations concluded that these systems are Mott insulators with antiferromagnetic ordering, where a spin-1/2 localized on each dimer. Of these reports, one  $\mu\text{SR}$  measurement has revealed a long-range antiferromagnetic

ordering with  $T_N = 39.3$  K in  $\beta^{\pm}\text{Me}_4\text{P}[\text{Pd}(\text{dmit})_2]_2$  compound. In the experiment, three signals were detected, which were presumed to be at the inequivalent sulfur atoms, consisting of thiol, thiolate, and thione moieties; elucidating the motivation for our research endeavors.

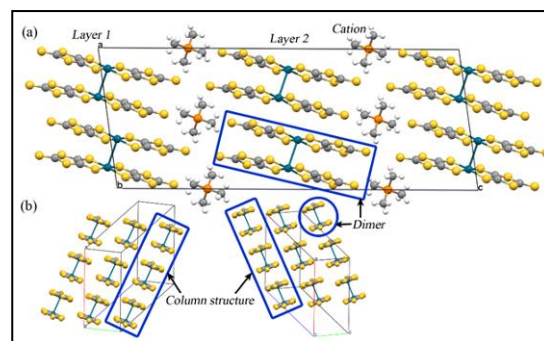


**Fig. 1.** (a) Unit cell of  $\beta^{\pm}\text{Me}_4\text{P}[\text{Pd}(\text{dmit})_2]_2$ . (b) Solid-crossing column structure of  $\beta^{\pm}\text{Me}_4\text{P}[\text{Pd}(\text{dmit})_2]_2$ .

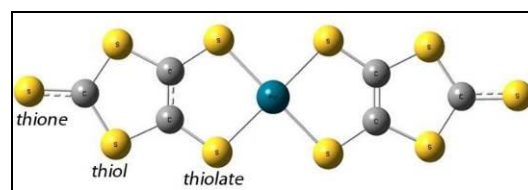


**Fig. 2.** Three inequivalent sulfur sites, consisting of thione, thiol, and thiolate.

b)  $\kappa\text{-(BEDT-TTF)}_2\text{Cu}[\text{N}(\text{CN})_2]\text{Cl}$  and  
 $\kappa\text{-d8-(BEDT-TTF)}_2\text{Cu}[\text{N}(\text{CN})_2]\text{Br}$

Organic charge transfer salts  $\kappa\text{-(BEDT-TTF)}_2\text{Cu}[\text{N}(\text{CN})_2]X$  ( $X = \text{Cl}, \text{Br},$  and  $\text{I}$ ), abbreviated as  $\kappa\text{-ET}$ , have gathered much attention due to their great potential application in spintronic devices. Their properties which are tunable with respect to lattice parameters also lead  $\kappa\text{-ET}$  to be the preference to both experimental and theoretical researchers. They exhibit various type of behaviors including superconducting, magnetic, and Mott insulating properties.  $\kappa\text{-ET}$  also possess other important properties such as spin liquid phase which depends on the temperature, pressure and the anion

part.

This research focuses on  $\kappa$ -(BEDT-TTF)<sub>2</sub>Cu[N(CN)<sub>2</sub>]Cl and  $\kappa$ -d8-(BEDT-TTF)<sub>2</sub> Cu[N(CN)<sub>2</sub>]Br abbreviated as  $\kappa$ -Cl and  $\kappa$ -d8-Br respectively, as they exhibit AFM configurations on the ground state. These compounds are organic magnet materials, which is similar to the materials in 1 (a). However, they are different in terms of the localized unpaired electron spin, which in this case is distributed throughout the cation.

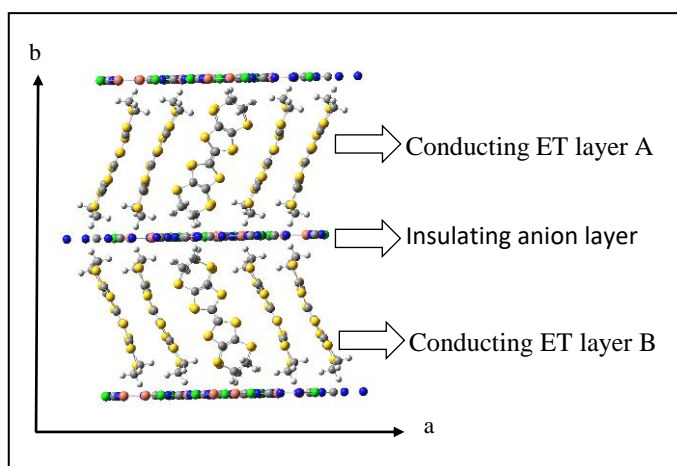


**Fig. 3.** Insulating and conducting layer of  $\kappa$ -(BEDT-TTF)<sub>2</sub>Cu[N(CN)<sub>2</sub>]X, with (ET=-(BEDT-TTF)<sub>2</sub>)

### ii. High-T<sub>c</sub> superconducting oxides

In this category, we are interested in two systems, La<sub>2</sub>CuO<sub>4</sub> (LCO) and YBa<sub>2</sub>Cu<sub>3</sub>O<sub>6</sub> (YBCO). Both systems are strongly correlated Mott insulators. Although those systems have been well investigated by  $\mu$ SR in the previous FY 2018 project, there still are a lot of experimental data required to be tested by the DFT investigations. The important points of this theme are to investigate the quantum effects of the muon itself and the spin states in the systems. We are currently investigating the spatial distributions of the muon itself around a stopping position due to zero-point vibration of the muon as a

light particle. We are also investigating the spatial distribution of the electron spins due to strongly hybridized electron orbitals which is the fundamental behavior in these strongly correlated systems. By considering the quantum effects, we expect our computational results to concur with the  $\mu$ SR experimental results. This finding can also be applied to another strongly correlated system to investigate their electronic state.

### iii. Short strand DNA

Deoxyribonucleic acid (DNA) is a versatile molecule that stores genetic information and consists of two polynucleotide chains twisted around each other in the form of a double helix. DNA is formed using sequences of four nitrogenous bases. These four bases are guanine (G), adenine (A), cytosine (C) and thymine (T). DNA nitrogenous bases are considered as aromatic compounds that are electron rich in nature. DNA bases provide an effective medium for electron transport because of the overlap in the electron orbital of adjacent bases. This study is divided into two parts which are an experimental investigation by using  $\mu$ SR experiment and computational investigation.

For the first-principle computational studies, the hyperfine coupling constant (HFCC) of muon at all possible Mu sites in the four nucleobases and four nucleotides have been investigated. The difference between nucleobases and nucleotides structures is that for the former a methyl group is attached to the nitrogenous base whereas for the later a sugar phosphate group is attached (see Fig. 4). According to the previous study, the use of a methyl group to replace sugar phosphate group can be a justifiable approximation as it can mimic the effect of the sugar phosphate group through

hyperconjugation effects. However, a methyl group is an electron donating group that could increase electron donating properties of the molecule. The question on the effect of a methyl group and a sugar phosphate group to the electronic structure and the hyperfine interaction of the nitrogenous base is, therefore, the motivation of this study.

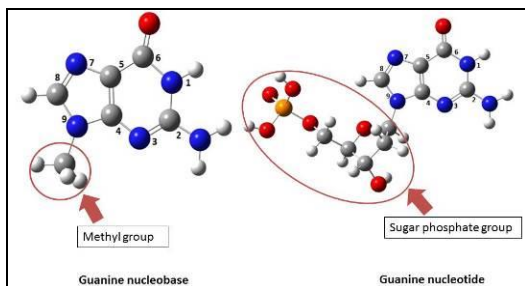


**Fig 4.** Guanine nucleobase and nucleotide structures.

These calculations were then extended to a 12mer homogenous single strand DNA. The length of the DNA oligomers was designed to be 12 because it is the length of a complete one turn of the double helix DNA structure and computationally compatible. Four systems which are short single strand DNA oligomers have been built in the following forms (Fig. 5):

- 1) 12mer single strand DNA oligomer with base sequence AAA... (adenine)
- 2) 12mer single strand DNA oligomer with base sequence TTT... (thymine)
- 3) 12mer single strand DNA oligomer with base sequence CCC... (cytosine)
- 4) 12mer single strand DNA oligomer with base sequence GGG... (guanine)

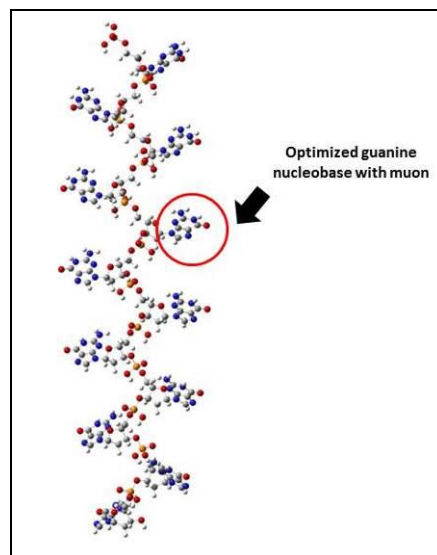


**Fig. 5.** 12mer single strand guanine

The results obtained from these calculations will be further studied and discussed in relation to the experimental work. For the experiment, we have also prepared the four 12mer oligomer samples. The double helix structure will be studied after the completion of calculations for the single strand systems. Therefore, the changes in the electronic structures as the structure of the systems changes can be examined from the computational and experimental studies on the electron dynamics, muon positions, and muon hyperfine interactions.

#### iv. Organic superconductors, $\lambda$ -(STF) $_2$ FeCl $_4$

The quasi-two-dimensional molecular organic magnet,  $\lambda$ -(BETS) $_2$ FeCl $_4$ , has been of interest since they host a  $\pi$ -d interacting spin system between the BETS  $\pi$ -conducting layer and Fe $^{3+}$  magnetic ion in the FeCl $_4$  insulating layer. This interaction with the direction parallel to the conducting layer can be compensated by the external magnetic field, resulting in a superconducting state in the field above 17 T. At the zero-field, the metal-antiferromagnetic insulator transition occurs at TAF(BETS) = 8.3 K. Despite that,

there has been a long debate regarding the mechanism of the antiferromagnetic state, namely, which spin is the driving force of the ordered state, the  $\pi$  or the d-spin?

It has previously been ascribed that  $\lambda$ -(STF)<sub>2</sub>FeCl<sub>4</sub> is located in the lower pressure region compared to  $\lambda$ -(BETS)<sub>2</sub>FeCl<sub>4</sub>. The TAF(STF) of this material determined by <sup>1</sup>H NMR was found to be 16 K without any anomaly observed in the temperature dependence of the spin susceptibility, arising from the 3d spins of the Fe<sup>3+</sup> ion. In addition, for the external field parallel to the c axis, there was a broad peak structure in the magnetic susceptibility at 8 K, coinciding with the TAF(BETS). Hence, it was suggested that TAF(STF) is due to AF long-range ordering in the  $\pi$ -spin system. In order to obtain direct evidence of the long-range ordering state below TAF(STF), zero-field (ZF)  $\mu$ SR measurements were conducted for the first time on randomly aligned  $\lambda$ -(BEDT-STF)<sub>2</sub>FeCl<sub>4</sub> crystals at the GPS beamline in Paul Scherrer Institute, Switzerland.

In conjunction with the  $\mu$ SR results, DFT calculations have been performed at the electronic minimum potential to determine the muon sites in  $\lambda$ -(STF)<sub>2</sub>FeCl<sub>4</sub>. Once the muon sites were determined, we aim to examine the spin distributions on the muon sites. The prediction of the spin distributions can be very valuable to calculate the dipole field of each site, and thus will allow us to compare the calculated values with the internal fields obtained from the experimental data.

#### v. Alkali metal superoxide

Spin-orbit coupling (SOC) in Mott insulators is an interesting physical phenomenon that has been intensively

investigated in the last decade. As an informative material, alkali-metal superoxides  $AO_2$  ( $A = \text{Na, K, Rb, Cs}$ ) present an interesting playground to examine the electromagnetic properties on the basis of  $p$ -electrons. This series of superoxides have been synthesized in the 1960s. Despite nearly a half-century since the first discovery of those systems, there are few studies on those magnetic properties. This is due to the difficulties of the synthesis and their high reactivity with the surroundings. One attractive feature of these alkali-metal superoxides is that the magnetic properties are well affected by changes in the lattice symmetry. It has been argued that magnetic structures significantly affected by the relative orientation of  $O_2^-$  species within the crystal lattice. In addition to this, the changes in the structure and magnetic properties depend on the alkali-metal ion. For that reason, systematic investigation on magnetically ordered states of  $AO_2$  is very important to reveal the overall magnetic scheme of the superoxides. The goals of this project are to determine the magnetic spin structure of alkali metal superoxides, their electronic states and the effect of SOC. According to Riyadi et al. (2012), there is a structural phase transition in  $CsO_2$ . The crystal structure of  $CsO_2$  is tetragonal at room temperature where the  $O_2$  molecular bond axes are parallel to the z-axis, while at low temperature the  $O_2$  molecular bond axes seem to tilt uniformly by 5°, leading to a lower symmetry orthorhombic structure. It is expected that there is a strong correlation between the structural phase transition and magnetic exchange interaction in  $CsO_2$ . Therefore, in our preliminary study, we have investigated the magnetic and electronic properties in the low symmetry structure of

CsO<sub>2</sub> using the computational method.

#### vi. Gold nanoclusters, [Au<sub>25</sub>SR<sub>18</sub>]

Thiolate protected Au nanoclusters have recently attracted significant research interest due to their fundamental physics as well as practical applications in the nanocluster technology. Metal nanoclusters refer to nano-sized M<sub>n</sub> clusters with a diameter of less than 2 nm. Recent advances in controlled syntheses show that the exact number of core atoms and ligands of very small metal nanoparticles can be regulated, referred to as “clusters”. These nanoclusters display interesting optical properties such as intense photoluminescence, which arises from discrete electronic energy level transitions that are available only in such extremely small particles. These properties have made the clusters different than the metal nanoparticles or even their bulk metals. Therefore, due to this reason, it is considered that the fractionated gold nanoclusters are molecular in nature.

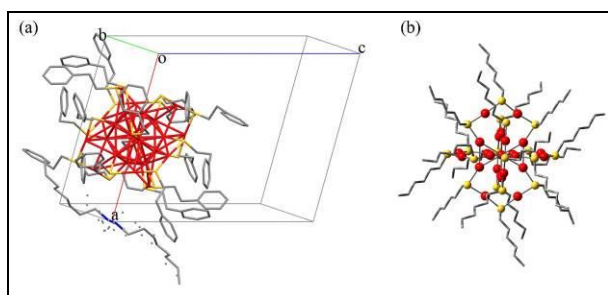


**Fig. 6:** (a) Unit cell Au<sub>25</sub>(SR)<sub>18</sub>N(C<sub>8</sub>H<sub>17</sub>)<sub>4</sub> (b) Structure of Au<sub>25</sub>(SR)<sub>25</sub>.

Typical gold nanoclusters may contain from 12 to 250 Au atoms with 144 being the size that borders between bulk and nanocluster in relation to the distinction in properties. Au<sub>25</sub> is considered the optimum size to exhibit magnetism due to the odd number of electrons that leads to an unpaired

spin in the system. Figure 6 (a) shows the unit cell of Au<sub>25</sub>(SR)<sub>18</sub>N(C<sub>8</sub>H<sub>17</sub>)<sub>4</sub> and the structure of Au<sub>25</sub>(SR)<sub>18</sub> is shown in Fig. 6(b). The reports on the magnetic properties of thiolate protected gold nanoclusters Au<sub>25</sub>SR<sub>18</sub>, however, are conflicting, where different magnetism has been concluded for the nature of the cluster, and hence, has become the motivation for our studies. The main objective of this research is to study the electronic and magnetic properties by implementing the muon technique using First-Principles DFT cluster method, hoping that it can serve as a benchmark, particularly in the magnetism studies.

#### 2. Specific usage status of the system and calculation method

Linear combination of atomic orbital molecular orbital (LCAO-MO) calculations were performed with the Gaussian16 program to study the electronic structure of the target systems. Aside from Gaussian16, VASP software was also used for the band structure calculations. The ADF software has also been employed in our computational work since it is known to provide better results on the hyperfine coupling constants. Thus far, we have utilized almost half of the allocated core time for GWMPD and BWMPD resources.

In FY 2018 project, only one user with user name = Dita1207 has applied for ACSG and ACSL resources. To date, both resources have been fully utilized.

The results obtained from the calculations by using all the resource units prove that HOKUSAI GreatWave supercomputer facility is very useful to perform the calculations, particularly on the large-scale systems. For the MPC resource unit, most of the core time utilized is intended to perform the calculations to determine the magnetic structures and electronic structures of muonated

target systems. These types of calculations, however, are considered to be very time-consuming. Due to the enormous amount of computational effort required to perform the calculations on the target systems, we need to apply more allocated core times for MPC.

### 3. Results

A considerable amount of computational effort has been done in FY2018 on the different systems, described in section 1. The data from the computational studies is accumulated to assist the interpretation of  $\mu$ SR experiments. The results for each subproject are reported separately and are as follows:

#### i. Organic magnets

The organic magnets consist of two classes of materials, (a)  $\beta'$ -X[Pd(dmit)<sub>2</sub>]<sub>2</sub>, and (b) (BEDT-TTF)<sub>2</sub>X systems, which share some similar properties. The implementation of these organic systems has been divided into two subprojects. The results for each class of materials are presented separately as follows:

##### a) $\beta'$ -X[Pd(dmit)<sub>2</sub>]<sub>2</sub>.

We have successfully determined the electronic as well as magnetic structures by employing the First-principles density functional theory cluster method. The results have been recently published in the Journal of the Physical Society of Japan. The detailed description of the results is explained in the publication entitled "First-principle studies of the magnetic structure and exchange interactions of  $\beta'$ -Et<sub>n</sub>Me<sub>4-n</sub>Z[Pd(dmit)<sub>2</sub>]<sub>2</sub>". Please find the attached publication.

The next endeavor has been focused on the effect of polarization function on the spin contamination and distribution in  $\beta'$ -Me<sub>4</sub>P[Pd(dmit)<sub>2</sub>]<sub>2</sub>. It was found that the

inclusion of polarization function in the calculations has resulted in the shifting of electron density from the sulfur atoms to the central Pd atoms. We have also found a peculiar inhomogeneity in the charge and spin distribution among the "dmit" groups in one formula unit. The structure is shown in Fig. 7. The calculations were carried out using the ONIOM method. The results have been presented at the International Conference on Functional Materials Science (ICFMS) 2018 in Bali, Indonesia and submitted for publication to the Key Engineering Materials Journal.

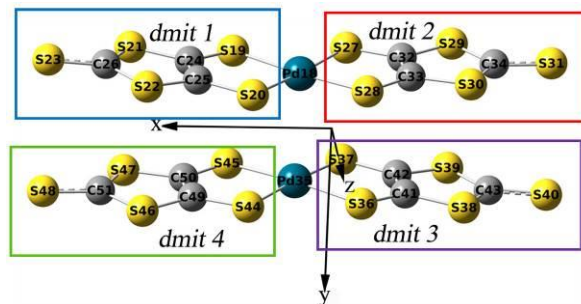


**Fig. 7:** [Pd(dmit)<sub>2</sub>]<sub>2</sub><sup>-</sup> dimer showing the labelling scheme for the *dmit* groups and individual atoms. The rectangle represents the region for each *dmit* group.

For the muonated systems, we present our results using  $\beta'$ -Me<sub>4</sub>P[Pd(dmit)<sub>2</sub>]<sub>2</sub> compound to represent the  $\beta'$ -X[Pd(dmit)<sub>2</sub>]<sub>2</sub> systems in which the results were then compared with the  $\mu$ SR experiments. We started our preliminary study with the muonated one-fragment cluster of  $\beta'$ -Me<sub>4</sub>P[Pd(dmit)<sub>2</sub>]<sub>2</sub>. The detailed descriptions of the results on the systems are explained in the publication entitled "Electronic Structure of Muonated Me<sub>4</sub>P[Pd(dmit)<sub>2</sub>]<sub>2</sub>". Now, we are focusing on the muonated systems in the antiferromagnetic state. For this case, we are now working on the dipole field calculations and, in the preparation, to submitting for

publications.

- b)  $\kappa$ -(BEDT-TTF)<sub>2</sub>Cu[N(CN)<sub>2</sub>]Cl and  
 $\kappa$ -d8-(BEDT-TTF)<sub>2</sub>Cu[N(CN)<sub>2</sub>]Br

For the last fiscal year, we have reported the results of DFT calculations on the non-muonated  $\kappa$ -Cl and  $\kappa$ -d8-Br. As for this fiscal year, we have performed the calculations on the muonated  $\kappa$ -Cl. There are four inequivalent muon positions in this study; S1, S3, C7 and C9. S1 is an outer Sulfur atom, while S3 is an inner sulfur atom. C7 and C9 are C = C inside the rings and at the center of the monomer, respectively. The computed results disclose that the geometrical parameters for S1 site possess the highest percentage difference, followed by S3, C7 and C9 site. Bond length between muonium and atom attached to it (S1, S3, C7 and C9) was found to be longer up to 56 % after optimization. This can be explained by perturbations affected by the addition of the muonium.

In terms of relative energy, S1 site was found to be the most stable site as compare to other sites. This is shown in Table 1 below.

**Table 1:** Relative energy for  $\kappa$ -Cl at S1, S3, C7 and C9 sites. The relative energy (eV) is taken with respect to S1 site.

	Relative energy	
	B3LYP	O3LYP
S1	0.000	0.000
S3	0.023	0.020
C7	0.044	0.039
C9	0.043	0.037

**Table 2:** Hyperfine coupling constant (in Gauss) for  $\kappa$ -Cl at S1, S3, C7 and C9 sites using computed using Gaussian and ADF software.

	Gaussian		ADF	
	B3LYP	O3LYP	B3LYP	O3LYP
C7	13.57	11.53	59.86	55.24
C9	-3.48	-2.56	53.72	46.81
S1	0.33	0.33	33.55	23.01
S3	-2.74	-1.62	43.34	31.99

From the  $\mu$ SR experiment, they observed two signals with the values of internal field: 58.4 G and 42.9 G. From the values of muon hfcc shown in the Table 2 above, the values of hfcc computed using ADF software at the B3LYP and O3LYP level of theory for S1 and S3 are the closest to the observation from experiment. It yields a hyperfine coupling constant with a percentage difference of 2.5% and 1.0% for C7 and S3, respectively. A very large difference is noted for all four muon sites calculated using Gaussian 16.

## ii. High-Tc superconducting oxides

### a) La<sub>2</sub>CuO<sub>4</sub>

In this study, the density functional theory (DFT) method within the supercell framework was employed (via the VASP software) to determine the possible muon sites in LCO. This information gives us a deeper understanding of the electronic states in its magnetically ordered state. The Coulomb repulsion of  $U = 8$  eV and the exchange parameter  $J = 0.8$  eV have been applied. Antiferromagnetic insulating behavior with  $0.61 \mu_B$  and an insulating gap of 1.9 eV was observed. This value is in a good agreement with previous experimental results. From the electrostatic potential calculations, we found

that there are three minimum potential points, as shown in Fig. 8. We named these points as M1, M2, and M3.

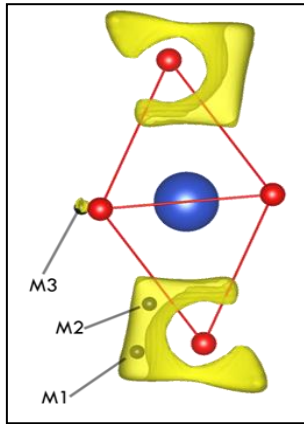


**Fig. 8.** Three possible muon positions (M1, M2, and M3) estimated by the electrostatic potential calculations.

In the subsequent calculations, one muon, which effectively acts as a positively charged dilute impurity, was introduced into a supercell structure to provide a realistic description of the systems. Fig. 9 shows the density of states (DOS) results obtained from different sized supercell. The DOS remain relatively constant as expected from the periodic boundary conditions implemented on the DFT calculations. Moreover, the same results were obtained for the muon local minimum positions, where no significant changes were observed for the M1, M2, and M3 positions.

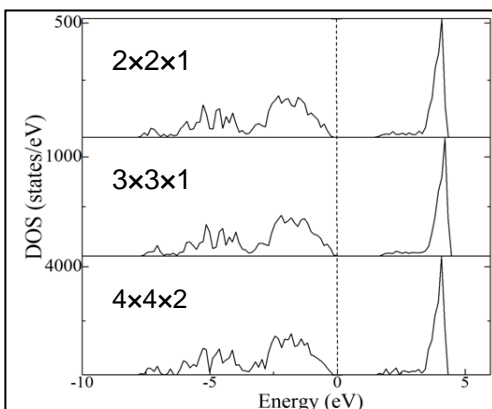


**Fig. 9.** Density of states of LCO for the 4-unit, 9-unit and 32-unit supercells.

By including one muon at each of the minimum positions, we can observe the local deformations on the crystal structure and its spin structure. The local deformations on the crystal and spin structure are similar for all supercell sizes that were considered. The largest supercell that consists of 32-unit cells is considered to be more accurate in terms of capturing the muon behavior inside the supercell. Fig. 10 shows how the implanted muon at position M2 affects the spin structure, as drawn at the  $\text{CuO}_4$  plane in the middle of the system. A slight reduction in the magnetic moment of the nearest Cu atom caused by the presence of muon affects the spin density of oxygen atom in the  $\text{CuO}_4$  plane. However, the antiferromagnetic behavior is preserved in the system as the deformation happens locally.

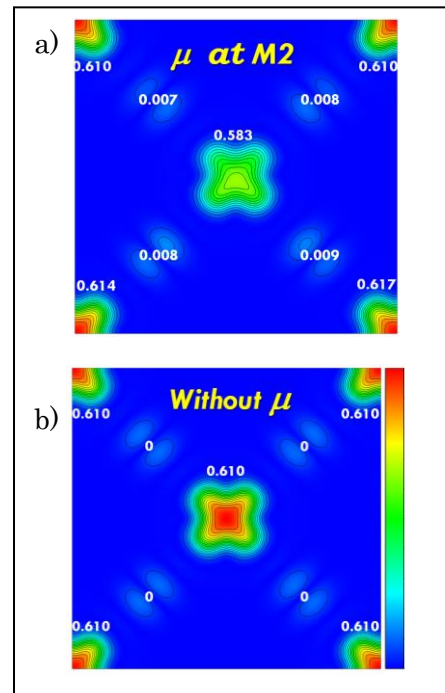


**Fig. 10.** Spin densities map of the  $\text{CuO}_4$  plane (a) with muon and (b) without muon. The white inscription gives an estimated value on each atom's magnetic moment.

b)  $\text{YBa}_2\text{Cu}_3\text{O}_6$ 

The density functional theory (DFT) calculations have been performed for YBCO using the VASP software. The first step is to reproduce the Mott insulator behavior in the ground state. We performed our calculations by using the generalized gradient approximation (GGA) with Perdew formulation, adding the additional Hubbard interaction  $U$ . We tuned the  $U$  values to open the band gap around the Fermi level, which play a key role to control the Mott insulator behavior.

As the muon carries a positive charge, it prefers to stop at the most minimum potential. The potential calculations that employ the DFT method estimate three different minimum potentials, which can be regarded as the initial muon positions. We also found that the muon position is not affected by the changing of the  $U$  value, whereas the calculated magnetic moment and size of the energy gap have a very strong dependence on the  $U$  value.

The calculated internal fields at the muon site were performed by considering the zero-point energy vibration and muon perturbation at each muon site. This calculation is based on the dipole-dipole interaction between muon and spin state of the system. The results show that the calculated value using an ionic picture of magnetism, where the spin resides in the particular ion overestimates the internal fields at the muon site. Therefore, we consider that as the covalency effect, which has a strong hybridization between the  $3d$  Cu orbital and the neighboring  $2p$  O orbitals. This effect causes the extended spin distribution in the real space, as shown in the Fig. 11.

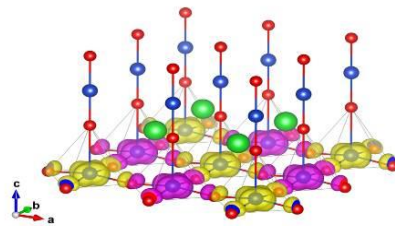


**Fig. 11.** Spin density  $\text{CuO}_2$  plane from DFT+ $U$  calculations. The magenta and yellow isosurfaces indicate the antiferromagnetic ordering. The  $p$  and  $d$  orbital characteristics are clearly visualized.

Subsequently, we calculated the internal fields at the muon site using spin density from our DFT+ $U$  calculation. Since the spin-density has a very strong dependence on the  $U$  value, we found that the internal field at the muon site also has a very strong dependence on the  $U$  value, as shown in the Table 3. The smallest difference between the experimental and calculated value obtained is by setting  $U = 6$  eV.

**Table 3.** The calculated internal fields (G) at the muon site on the basis of spin-density calculations

U (eV)	Muon Position M1 (G)	Muon Position M2(G)	Muon Position M3 (G)
0	16.34	48.58	37.42
1	5.60	62.45	62.24
2	27.93	69.20	119.99
3	24.11	84.38	111.94
4	24.59	254.82	169.06
5	42.60	284.26	206.50
6	45.97	316.64	223.96
7	49.35	324.69	241.15
8	52.51	347.05	249.74
9	56.05	348.99	258.36
10	58.09	386.30	288.23
11	61.20	408.05	303.73

Exp.Value	117.7	295.5	220.4
-----------	-------	-------	-------

We have already submitted the preliminary results to the Key Engineering Journal. "Magnetic Properties of  $\text{YBa}_2\text{Cu}_3\text{O}_6$  Studied by Density Functional Theory Calculation". In the upcoming fiscal year, we plan to clarify the hyperfine interactions at each muon site. These interactions are caused by the overlapping of the spin-density with the muon wavefunction. We are now preparing the manuscript, which includes the covalency effect while waiting for the hyperfine calculation results.

### iii. Short strand DNA

The converged molecular orbitals were used to examine the electronic structures of the systems and the muon hyperfine coupling constant (HFCC) at each possible muon site. The calculation was started with the nucleobase and then followed by the nucleotide structures.

For the electronic structure investigation, all optimized structures preserved the planar geometrical shape of the nitrogenous bases after atomic relaxation. The addition of methyl group or sugar phosphate group results in similar effects to the bond lengths and bond angles. The changes in bond lengths and bond angles do not result in any significant modification to the planar shape of the nitrogenous bases. The existence of the methyl group and the sugar phosphate group does not give any significant effect to the charge distribution around the nitrogenous bases ring. Structures with a sugar phosphate group attached to the nitrogenous base have a larger HOMO-LUMO gap. Hence, it is clear that the inclusion of a sugar phosphate group has an impact on the HOMO-LUMO gap. The

changes in the HOMO-LUMO gap could affect the possibilities of charge transport through DNA. Thus, from our computational study, the presence of a methyl group or a sugar phosphate group to the nucleic acid bases has a direct effect on the structure of the system.

The effects of split valence basis sets on the muon hyperfine interaction in guanine nucleobase and nucleotide structures have been studied. The quality of calculations depends on the theoretical method and the basis set of Gaussian function chosen. The aim of this study is to examine quantitatively the changes in the calculated hyperfine interactions due to basis set effects. Guanine in nucleobase and nucleotide form were chosen as the models in this study. Fig. 12 shows the deviation of Fermi contact value calculated using different basis sets.

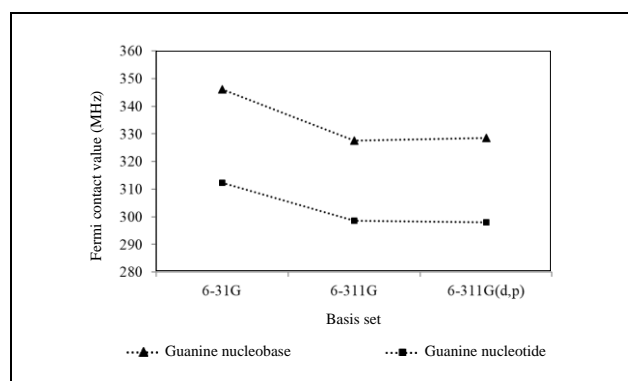


**Fig. 12.** Deviation of Fermi contact value calculated using different basis sets.

The results from this current work have been presented at the international conference as listed in the List of Publication section of this report.

Currently, the computational work to obtain the electronic structure 12mer single strand DNA oligomer for adenine, guanine, thymine, and cytosine has been initiated. As

the number of electrons in the single strand DNA oligomer is 12 times larger than the single nucleotides it takes a much longer computing time to perform the calculation. The total number of electrons in the 12mer single strand DNA oligomers are 1,955, 1,811, 1,907 and 2,051 for A, C, T, and G respectively. Therefore, the computational work to investigate the electronic structure and muon trapping sites with the associated HFCC at other nucleotides especially the terminal ones is still in progress.

#### iv. Organic superconductors, $\lambda$ -(STF) $_2$ FeCl $_4$

##### a. Determining the stable crystal structure

The unit cell of  $\lambda$ -(STF) $_2$ FeCl $_4$  that consists of 4 STF molecules and 2 FeCl $_4$  molecules, has 114 atoms in total. In one STF molecule, there are 6 S (sulfur) atoms and 2 Se (selenium) atoms. However, the x-ray diffraction is unable to determine the exact position of Se atoms in the center of STF molecule. Therefore, it leads to a slight distortion of the crystal structure, as shown in Figure 13(a). DFT calculations were performed to study the muon sites. For the initial step, we need to determine the stable crystal structure. Figure 13(b) shows the result of the stable crystal structure after several simple electrical minimum potentials for each single STF molecule were examined. The optimum Se and S atomic positions were selected based on the results from the minimum energy obtained from the DFT calculations.

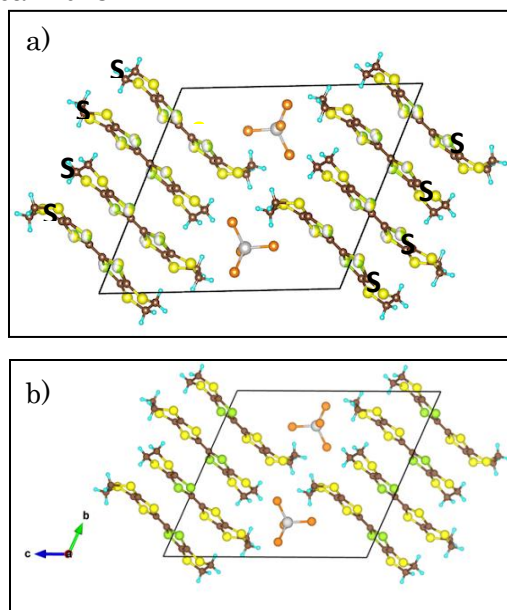


**Fig. 13.** (a) Original crystal structure of  $\lambda$ -(STF) $_2$ FeCl $_4$  determined from x-ray diffraction. There is a 50% occupancy of the S and S atoms in the center of STF molecule. (b) The stable crystal structure determined by DFT calculation. The so-called zig-zag configuration of selenium atom obtained from the lowest energy after a converged electrical minimum potential calculation.

##### b. Determination of the muon stopping sites

The stable crystal structure obtained from the previous calculations was used to calculate the electrical minimum potential. From the calculation, two different sites were observed in the isosurface area, covering up to 100 meV of potential energy. It is noted that the observations from theoretical calculations are consistent with the one from  $\mu$ SR experimental results. Remarkably, the sites are quite well separated. One of the muon site is close to the Fe $^{3+}$  ion and another one is close to the H atom at the edge of STF molecule.

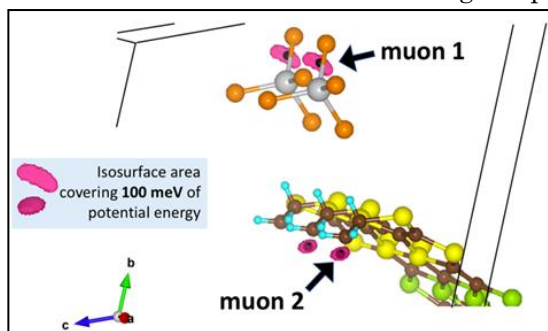


**Fig. 14.** The two muon stopping sites in  $\lambda$ -(STF) $_2$ FeCl $_4$ . One site is close to the Fe $^{3+}$  ion and the other one is close to the H atom in the STF molecule.

#### v. Alkalimetal superoxide

Fig. 15 displays the minimum potential positions in CsO $_2$  estimated from DFT calculations as implemented in the VASP software are described by the iso-surface areas with the exact energy region from the potential minimum positions (yellow surface). There are two possible muon positions around the O $_2^-$  dumbbell, which are labelled as M1 and M2. For the exchange-correlation potential, the generalized gradient approximation (GGA) was used. We also incorporate the on-site Coulomb Interaction ( $U$ ) between the oxygen  $2p$  electrons. Dark marks in those extracted figures indicate the exact locations of the local minimum potential. These local minimum positions can be regarded as the initial stopping sites for the injected muons. Two different muon positions were revealed in the current study around the oxygen dumbbell. Those different sites are caused by the titling of the oxygen dumbbell against to the  $c$ -axis. Assuming the system has the same AF spin structure with the one observed in KO $_2$ , we found two probable muon sites in the vicinity of the dumbbell oxygen, namely (0.7373; 0,2500;0.5859) and (0.6999;0.2567;0.5762). We found that the muon stopped near an oxygen atom. This is because an injected

muon has a positive charge and preferentially stops close to the anions, which carry negative charges. The two-muon stopping positions have confirmed that our calculation results have a good agreement with the experimental results.

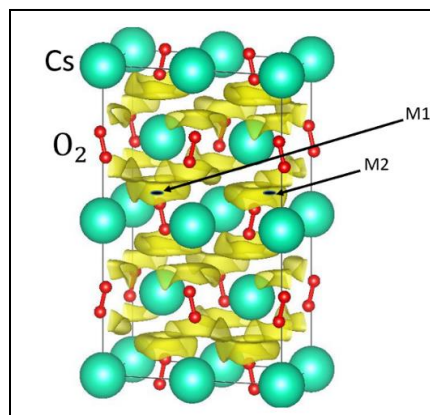


**Fig. 15.** Minimum potential positions estimated from the density functional theory (DFT) calculations. The yellow color represents the iso-surface areas that have the energy of 200 meV higher than the local minimum potential positions.

The results show that the on-site Coulomb interaction is important for the correct description of the insulating electronic structure of CsO $_2$  at the low symmetry phase. Fig. 16 shows the band structure and density of states in CsO $_2$ . The band structure obtained from the calculation results shows that the band gap opening occurs when applying the on-site Coulomb interaction of  $U=2$ .

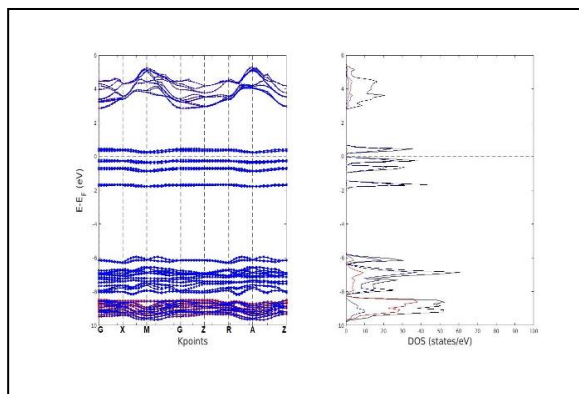


**Fig. 16.** Band structure and density of states in  $\text{CsO}_2$

vi. Gold nanoclusters,  $[\text{Au}_{25}\text{SR}_{18}]$

First-principles DFT studies of the electronic and magnetic structures in these gold nanocluster systems have been performed using the Gaussian 16 software package. At present, our study has been focused on the hyperfine interactions in  $\text{Au}_{25}\text{SR}_{18}$  with  $R = \text{hexyl}$  ( $\text{C}_6\text{H}_{13}$ ).

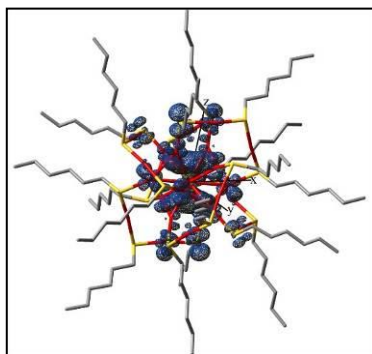


**Fig. 17.** Surface plot of spin densities for  $[\text{Au}_{25}(\text{SR})_{18}]^0$ .

Two oxidation states were considered, namely, 0 and -1. For the 0 cluster, the calculations were carried out at the doublet state, whereas the singlet state has been set for the -1 cluster. Figure 17 shows the surface plot of spin density distribution for the 0 cluster. The distribution of the electron spin density shows that the unpaired electron in the systems has the delocalized behavior.

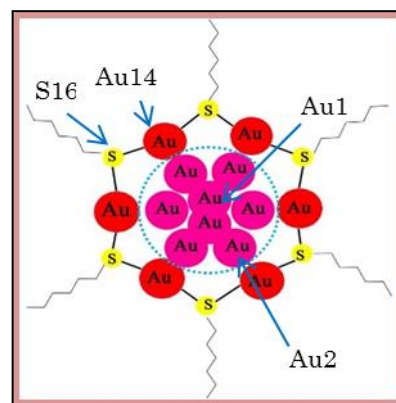


**Fig. 18.** Possible muon sites in  $\text{Au}_{25}\text{SR}_{18}$  ( $R_1 = \text{hexyl}$ ) with -1 and 0 oxidation states.

A total of four possible muon stopping sites in both oxidation states were found to be energetically stable, depicted in Table 4. The calculations were performed at the B3LYP/Def2SVP level of theory. We found the magnitude of the hyperfine interactions for every muon site is negative, which is attributed to the negative values obtained from the Fermi contact interaction.

**Table 4.** Relative energy for possible muon site within  $[\text{Au}_{25}(\text{SR})_{18}]^-$  and  $[\text{Au}_{25}(\text{SR})_{18}]^0$  nanocrystals. The relative energy refers to the energy of the system relative to the site that has the lowest energy. The lowest energy for the -1 system is at Au2 and S16 for the 0 system.

$[\text{Au}_{25}(\text{SR})_{18}]^-$		$[\text{Au}_{25}(\text{SR})_{18}]^0$	
Muon site	Relative Energy (eV)	Muon Site	Relative Energy (eV)
Au2	0.000	S16	0.000
Au14	0.093	Au2	0.110
S16	0.496	Au14	0.163
Au1	0.514	Au1	0.173

## 4. Conclusions

We have successfully carried out the computational work, which is the basis of our research efforts in studying the electronic and magnetic characteristics of these interesting target materials, particularly in the muon studies. The immense computing power of the HOKUSAI GreatWave supercomputer has provided an important contribution to our research efforts and enabled us to conduct a wide range of computationally intensive tasks in various materials. Some of the results obtained from our calculations have been successfully presented and published. However, there are some objectives for FY2018 have not yet been achieved, since the accurate results couldn't be attained due to their large scale as well as the complexity of the structures, especially for the muonated compounds. We wish to achieve those objectives in the near future. Therefore, more time is required, and it is of great importance for us to pursue our usage in HOKUSAI GreatWave supercomputer for FY2019. Each of our subprojects has its own specific targets and objectives, which have been achieved. The accomplishment of every subproject is comprehensively concluded as follows:

## i. Organic magnets

We have performed DFT calculations on the target systems by using Gaussian16 and ADF software. In the study of the pure systems, we have successfully determined their origin of magnetism, which is proved to be different than that of the conventional magnets. The magnetic structures of these organic magnets have been obtained using Heisenberg exchange interactions, adopting the broken-symmetry approach. We have also succeeded to estimate the muon stopping positions in these organic magnets. These results make it possible for us to make comparisons with  $\mu$ SR experimental

results. The conclusions for the two subprojects are presented as follow:

a)  $\beta'$ -X[Pd(dmit)<sub>2</sub>]<sub>2</sub>.

For the pure systems, some of the results have already been published in the Journal of the Physical Society of Japan and submitted to the Key Engineering Materials Journal. We are now preparing another manuscript on these pure systems and wish to submit it in April 2019.

Most computational works for these muonated systems were already completed except for two characterizations, the vibrational averaging for the muon hyperfine interactions as well as point dipole calculations. For the point dipole calculations, the accomplishment of this characterization is hampered by the complexity of the electronic structure of the systems. This is due to the delocalized nature of the unpaired electron distribution that characterizes the magnetism. Therefore, more computing time is needed for the accomplishment of this subproject.

b)  $\kappa$ -(BEDT-TTF)<sub>2</sub>Cu[N(CN)<sub>2</sub>]Cl and  $\kappa$ -d8-(BEDT-TTF)<sub>2</sub>Cu[N(CN)<sub>2</sub>]Br

There are four inequivalent muon positions were considered in this study; S1, S3, C7 and C9. The computed results disclose that the geometrical parameters for S1 site possess the highest percentage difference, followed by S3, C7 and C9 sites. From the calculated relative energy, we found that S1 site is the most stable site compare to others. The values of HFCC computed using ADF software at the B3LYP and O3LYP level of theories for S1 and S3 are the closest with the experiment. The difference percentage values of 2.5% and 1.0% were obtained for S1 and S3, respectively. However, a very large difference is noted for all four muon sites calculated

using Gaussian 16.

ii. High-Tc superconducting oxides

a)  $\text{La}_2\text{CuO}_4$

The antiferromagnetic insulating behavior as well as the insulating gap observed are in a good agreement with previous experimental results. From the electrostatic potential calculations, three minimum potential points were found, which were labelled as M1, M2, and M3. All the muon positions are energetically stable upon introducing the muon in the different sized supercell structures. The antiferromagnetic behavior is preserved in the system as the deformation happens locally.

b)  $\text{YBa}_2\text{Cu}_3\text{O}_6$  (YBCO6)

The preliminary results of our investigation were already integrated and submitted to the Key Engineering Materials Journal.

From the results, it can be concluded that the muon position is not affected by the changing of the U value, whereas the calculated magnetic moment and size of the energy gap have a very strong dependence on the U value.

The internal fields at muon site in YBCO6, which include local crystal deformations due to the presence of muons and quantum nature of implanted muons were determined. The local perturbation and zero-point energy of muon were also considered when elucidating the  $\mu\text{SR}$  results and Cu-spin state.

iii. Short strand DNA

DFT cluster method was successfully employed to investigate the electronic structures of guanine and cytosine in the nucleobase and nucleotide forms, using B3LYP/6-311++G (d,p) level of theory. From the computational study, we found that the presence of the methyl group or a sugar

phosphate group to the nucleic acid bases has a direct effect on the structure of the system. The planar structure of the nitrogenous base is maintained after geometry optimization procedure. No significant difference was found in the charge distribution in nucleobase and nucleotide forms for both guanine and cytosine. The ionization energy for guanine is found to be lower than that for cytosine. The HOMO-LUMO gap is lower for both guanine and cytosine in the nucleobase form. The calculated dipole moment shows that guanine is more polarized than cytosine. From the computational study, the presence of a methyl group or a sugar phosphate group to the nucleic acid bases has a direct effect on the structure of the system.

iv. Organic superconductors,  $\lambda$ -(STF) $_2$ FeCl $_4$

From the Zero Field  $\mu\text{SR}$  study of  $\lambda$ -(BEDT-STF) $_2$ FeCl $_4$ , it is found that there are two distinct internal fields from the fast and slow frequency of the muon spin precession. We also found two 2nd order phase transition around 16 K and 8 K, observed from the Asymmetry (T). The results are consistent with magnetization, NMR and Fe Mossbauer spectroscopy measurements. From the Relaxation Rate (T), the critical slowing down just above the  $T_N$ , however, is not so clear.

From the DFT calculations of the minimum electronic local potential, two possible muon stopping sites were determined. In this case, the first site is found to be close to the Fe atom, whereas the other one is close to the H atom at the edge of the STF molecules.

v. Alkali metal superoxide

Two probable muon sites in the vicinity of the dumbbell oxygen were found from the electrostatic potential calculations, employing the DFT method. This is due to

the negative charge on the oxygen atom that has the inductive effect towards the muon. The two-muon stopping position confirms that the calculation results have a good agreement with the experimental results, which show two internal fields at the muon site.

We also found that the correct description of the insulating electronic structure of CsO<sub>2</sub> and on-site Coulomb interaction are important for the low symmetry phase. Band structure calculations revealed that the band gap opening occurs by applying the on-site Coulomb interaction,  $U=2$ .

vi. Gold nanoclusters

From the spin density distribution for the pure system with 0 oxidation state, the system is found to have the delocalized electron behavior.

Four possible muon stopping sites in both oxidation states were found to be energetically stable, with the magnitude of the hyperfine interactions for each site is found to be negative. The objective for the muonated system has not yet been accomplished. We still need to calculate on the vibrational averaging to complete the hyperfine interaction results.

Our research activities using the Hokusai supercomputing facility in the FY 2018 have resulted in one published paper, five papers submitted and under review, and 18 oral and poster presentations at the international conferences.

5. Schedule and prospect for the future

On the basis of our achievements in 2018, we plan to perform more complex calculations on our target systems and try to gain the following goals. Although there are still some of our set goals that have not yet been achieved, we are positive that

they can be completed in a short time. For the new fiscal year project (2019), we expect to continue and perform more complex calculations on our target systems. More data from the calculations is expected to be published in 2019. Further description of our prospects is described in the research plan for 2019, which will be submitted to RIKEN after the submission of this report.

i. Organic magnets.

For this fiscal year (FY 2018), considerable interest has been devoted to a deeper investigation on the muonated system for both series of compounds, BEDT-TTF)<sub>2</sub>X and  $\beta^{\prime}$ X[Pd(dmit)<sub>2</sub>]<sub>2</sub> systems. Some of the results on the hyperfine interactions have successfully been acquired. However, due to the complexity of the electronic structure of these organic magnets, we require an extension of the core times, particularly for the point dipole and muon vibrational averaging calculations. Therefore, we wish that this subproject will be considered and included in the FY 2019 project, so that we will enable to complete the remaining computational work. This is important to obtain the accurate results for the muon hyperfine interactions. For the pure systems, more attention will be paid on the (BEDT-TTF)<sub>2</sub>X derivatives since the results on the magnetic structure of  $\beta^{\prime}$ X[Pd(dmit)<sub>2</sub>]<sub>2</sub> series have already been published.

ii. High-Tc superconducting oxides

For this fiscal year of 2019, we have planned to observe the Fermi contact field experienced by the muon using the large supercell systems. Furthermore, we also plan to do post-processing for our DFT calculations by using Wannier code to clarify the covalency effect on our systems. We will carry out the calculations on both La<sub>2</sub>CuO<sub>4</sub> and YBa<sub>2</sub>Cu<sub>3</sub>O<sub>6</sub>.

iii. DNA

We have obtained  $\mu$ SR experimental results on all four single strand DNA oligomer samples. Thus, we are now moving to the next stage on the basis of our findings on the single strand DNA model molecules by using computational results. Some of the present data have been presented at international conferences. We plan to publish  $\mu$ SR experimental and computational results on the single strand DNA molecules after all the computational calculations are completed.

iv. Organic superconductors,  $\lambda$ -(STF)<sub>2</sub>FeCl<sub>4</sub>

The main aim of this work is to continue the calculations for the supercell system in order to simulate the muon implantation in the crystal. In addition, the calculations on the collinear spin structure are also needed to assist the preliminary results obtained in the FY 2018 project. It is also important to calculate the dipole field for several spin structure configurations. The calculated results will then be compared with the measured internal fields from  $\mu$ SR experimental data. The underlying idea is to select the best spin structure for  $\lambda$ -(STF)<sub>2</sub>FeCl<sub>4</sub>.

ii. Gold nanoclusters, [Au<sub>25</sub>SR<sub>18</sub>]

For Au<sub>25</sub>SR<sub>18</sub> with R = hexyl, we still have some calculations to be completed, particularly in determining the muon vibrational averaging for the hyperfine interactions. At present, we are preparing a manuscript, focusing on the hyperfine interactions. This paper, however, does not include the vibrational averaging calculations. We intend to submit the manuscript to the Journal of Physical Society of Japan in February, whereas the one with the vibrational averaging is expected to be submitted in June 2019.

The next focus is on Au<sub>25</sub>SR<sub>18</sub> system with R = ethylbenzene. Aside from the muon studies, we also want to investigate more detail in bonding interactions particularly the aurophilicity effects on the two target systems, which possess different coordinating ligands. We are planning to prepare two more publications for these systems, which are expected to be released in August and October 2019.

As explained in detail above, we are planning to perform further and more complex calculations on our target systems. For the future project (FY2019), we would like to continue using both GW and BW resources in the HOKUSAI supercomputing facility as the powerful and large-scale calculations are required in our research endeavors.

**Fiscal Year 2018 List of Publications Resulting from the Use of the supercomputer**

**[Paper accepted by a journal]**

1. Ahmad S.N.A., Sulaiman, S., Ang, L.S., Watanabe, I. First-Principles Studies of the Magnetic Structure and Exchange Interactions of  $\beta'$ - $\text{Et}_n\text{Me}_{4-n}\text{Z}[\text{Pd}(\text{dmit})_2]_2$ , Journal of the Physical Society of Japan, 87 (2018) 124709. (ISI indexed)

**[Conference Proceedings]**

1. Ramli, I., Mohd-Tajudin, S.S., Ramadhan M.R., Mohamed-Ibrahim, M. I., Sulaiman, S., Sari, D.P., Kurniawan, B., Watanabe, I. Magnetic Properties of  $\text{YBa}_2\text{Cu}_3\text{O}_6$  Studied by Density Functional Theory Calculation. Submitted to Key Engineering Materials Journal. (In review)
2. Zaharim, W.N., Sulaiman, S., Abu Bakar, S.N., Ismail, N.E., Rozak, H., Watanabe, I. (September, 2018). Density Functional Theory Studies on Guanine and Cytosine. ICMR 2018 – 7<sup>th</sup> International Conference on Multidisciplinary Research. (In review)
3. Zaharim, W.N., Sulaiman, S., Abu Bakar, S.N., Ismail, N.E., Rozak, H., Watanabe, I. The Effects of Split Valence Basis Sets on Muon Hyperfine Interaction in Guanine Nucleobase and Nucleotides Structures. Submitted to Key Engineering Materials Journal. (In review)
4. Ahmad S.N.A., Sulaiman, S., Ang, L.S., Watanabe, I. Effects of Polarization Function on the Spin Contamination and Distribution in  $\beta'$ - $\text{Me}_4\text{P}[\text{Pd}(\text{dmit})_2]$ . Submitted to Key Engineering Materials Journal. (In review)
5. M. R. Ramadhan, I. Ramli, M. D. Umar, S. Winarsih, A. Manaf, B. Kurniawan, M. I. Mohamed-Ibrahim, S. Sulaiman, I. Watanabe. Effects of the Supercell Size on the Muon Site Calculations of  $\text{La}_2\text{CuO}_4$ . Submitted to Key Engineering Materials Journal. (In review)

**[Oral presentation]**

1. Dita Puspita Sari, R. Asih, S. Sulaiman, K. Hiraki, A. Hillier, H. Aizawa, T. Koretsune, H. Seo, K. Kuroki, T. Nakano, Y. Nozue, A. Yamamoto, I. Watanabe, and Y. Ishii. (November, 2018).  $\mu\text{SR}$  study of the admixture of an s-wave component into the d-wave superconducting gap symmetry in  $\lambda$ -(BETS) $_2\text{GaCl}_4$ . *Oral presentation at 4<sup>th</sup> ICFMS 2018 in conjunction with 2<sup>nd</sup> RIKEN Symposium: International Workshop on Organic Molecular System*. Bali, Indonesia.
2. Dita Puspita Sari, T. Minamidate, N. Matsunaga, A. Kawamoto, I. Watanabe, and Y. Ishii. (September, 2018). *Oral presentation at JPS Autumn Meeting 2018*. Kyoto, Japan.

## Usage Report for Fiscal Year 2018

3. Zaharim, W.N., Sulaiman, S., Abu Bakar, S.N., Ismail, N.E., Rozak, H., Watanabe, I. (September, 2018). Density Functional Theory Studies on Guanine and Cytosine. *Oral presentation at The 7<sup>th</sup> ICMR Conference 2018* (pp 51). Medan, Indonesia.
4. Dita Puspita Sari, R. Asih, S. Sulaiman, K. Hiraki, A. Hillier, H. Aizawa, T. Koretsune, H. Seo, K. Kuroki, T. Nakano, Y. Nozue, A. Yamamoto, I. Watanabe, and Y. Ishii. (August, 2018). The admixture of an s-wave component into the d-wave superconducting gap symmetry in  $\lambda$ -(BETS)<sub>2</sub>GaCl<sub>4</sub>. *Oral presentation at Gordon Research Seminar*. Rhode Island, US.
5. Dita Puspita Sari, R. Asih, K. Hiraki, T. Nakano, A. Hillier, H. Aizawa, T. Koretsune, H. Seo, Y. Nozue, A. Yamamoto, I. Watanabe, and Y. Ishii. (July, 2018). Superconducting gap symmetry of  $\lambda$ -(BETS)<sub>2</sub>GaCl<sub>4</sub> studied by  $\mu$ SR and DFT. *Invited talk at Muon Spectroscopy User Meeting: Future Developments and Site Calculations 2018*. Abingdon, United Kingdom.
6. Ramli, I., Mohd-Tajudin, S.S., Ramadhan M.R., Mohamed-Ibrahim, M. I., Sulaiman, S., Nishizaki, T., Kurniawan, B., Watanabe, I. (July, 2018). How muon senses ordered Cu spin in YBa<sub>2</sub>Cu<sub>3</sub>O<sub>6</sub>? - A supercell approach by DFT calculations. *Oral presentation at Muon Spectroscopy User Meeting: Future Developments and Site Calculations 2018*. Abingdon, United Kingdom.
7. M. R. Ramadhan, I. Ramli, A. Manaf, B. Kurniawan, I. Watanabe. (July, 2018). A Revisit to the Ordered State of Cu-Spins in La<sub>2</sub>CuO<sub>4</sub> Simulated by DFT – Quantum Approach to Muon Sites. *Oral presentation at the Muon Spectroscopy User Meeting: Future Developments and Site Calculations*. Abingdon, United Kingdom.
8. Ramli, I., Mohd-Tajudin, S.S., Ramadhan M.R., Mohamed-Ibrahim, M. I., Sulaiman, S., Nishizaki, T., Kurniawan, B., Watanabe, I. Study of Microscopic Magnetism in YBa<sub>2</sub>Cu<sub>3</sub>O<sub>6</sub> by  $\mu$ SR and DFT. (July, 2018). *Oral presentation at The 4<sup>th</sup> Emallia Conference 2018 Hokkaido Univ. - Pusan Univ. - RIKEN Symposium*. Sapporo, Japan.
9. M. R. Ramadhan, I. Ramli, M. D. Umar, S. Winarsih, B. Adiperdana, B. Kurniawan, M. I. Mohamed-Ibrahin, S. Sulaimanm T. Adachi, I. Watanabe. (July, 2018). Contribution of Quantum Effects on the Muon Site Calculation of La<sub>2</sub>CuO<sub>4</sub>. *Oral presentation at the 4<sup>th</sup> Emallia Conference 2018 Hokkaido Univ. – Pusan Univ. – RIKEN Symposium*. Sapporo, Japan.
10. J. Angel, H. Nomura, T. Taniguchi, K. Matsuhira, I. Watanabe. (July, 2018). Magnetically Ordered States in hole-doped pyrochlore iridate Y<sub>2</sub>Ir<sub>2</sub>O<sub>7</sub>. *Oral presentation at The 4<sup>th</sup> Emallia Conference 2018 Hokkaido Univ. - Pusan Univ. - RIKEN Symposium*. Sapporo, Japan.
11. Ramli, I., Mohd-Tajudin S.S., Mohamed-Ibrahim, M. I., Sulaiman, S., Watanabe, I. (February, 2018). Muon Sites in high-Tc Superconductor, YBa<sub>2</sub>Cu<sub>3</sub>O<sub>6</sub>. *Oral presentation at RIKEN AICS HPC Youth Workshop 2018*. Kobe, Japan.

## Usage Report for Fiscal Year 2018

12. Sulaiman, S. (February, 2018). DFT Studies on Muon Sites and Associated Hyperfine Interactions in Single Strand DNA. *Oral Presentation at URICAS Symposium 2018*. RIKEN, Japan.

### [Poster presentation]

1. M. R. Ramadhan, I. Ramli, M. D. Umar, S. Winarsih, B. Kurniawan, A. Manaf, M. I. Mohamed-Ibrahim, S. Sulaiman, I. Watanabe. (January, 2019). Quantum Effects of Muon on the Electronic State of  $\text{La}_2\text{CuO}_4$ . *Poster Presentation at the 1<sup>st</sup> NCKU-RIKEN Joint Workshop International Workshop on Topological Quantum Materials*. Tainan, Taiwan.
2. Sari D.P., Ramadhan M.R., Ramli, I., M. D. Umar, S. Winarsih, A. Manaf, B. Kurniawan, Mohamed-Ibrahim, M. I., Sulaiman, S., Watanabe, I. (November, 2018). Effects of the Supercell Size on the Muon Site Calculations of  $\text{La}_2\text{CuO}_4$ . Poster presentation at 4th ICFMS 2018 in conjunction with 2nd RIKEN Symposium: International Workshop on Organic Molecular System. Bali, Indonesia.
3. Ramli, I., Mohd-Tajudin, S.S., Ramadhan M.R., Mohamed-Ibrahim, M. I., Sulaiman, S., Kurniawan, B., Watanabe, I. (November, 2018). Covalent bonding effect on the magnetism of  $\text{YBa}_2\text{Cu}_3\text{O}_6$  studied by DFT and  $\mu\text{SR}$ . *Poster presentation at 4<sup>th</sup> ICFMS 2018 in conjunction with 2<sup>nd</sup> RIKEN Symposium: International Workshop on Organic Molecular System*. Bali, Indonesia.
4. M. R. Ramadhan, I. Ramli, M. D. Umar, S. Winarsih, A. Manaf, B. Kurniawan, M. I. Mohamed-Ibrahim, S. Sulaiman, I. Watanabe. (November, 2018). Effects of the Supercell Size on the Muon Site Calculations of  $\text{La}_2\text{CuO}_4$ . *Poster presentation at 4<sup>th</sup> ICFMS 2018 in conjunction with 2<sup>nd</sup> RIKEN Symposium: International Workshop on Organic Molecular System*. Bali, Indonesia.
5. Zaharim, W.N., Sulaiman, S., Abu Bakar, S.N., Ismail, N.E., Rozak, H., Watanabe, I. (November, 2018). The Effects of Split Valence Basis Sets on Muon Hyperfine Interaction in Guanine Nucleobase and Nucleotides Structures, *Poster presentation at 4<sup>th</sup> ICFMS 2018 in conjunction with 2<sup>nd</sup> RIKEN Symposium: International Workshop on Organic Molecular System*. Bali, Indonesia.
6. Ahmad, S.N.A., Sulaiman, S., Ang, L.S., Watanabe, I. (November, 2018). Effects of Polarization Function on the Spin Contamination and Distribution in  $\beta^{\text{e}}\text{Me}_4\text{P}[\text{Pd}(\text{dmit})_2]$ , *Poster presentation at 4<sup>th</sup> ICFMS 2018 in conjunction with 2<sup>nd</sup> RIKEN Symposium: International Workshop on Organic Molecular System*. Bali, Indonesia.
7. Ramli, I., Mohd-Tajudin, S.S., Ramadhan M.R., Mohamed-Ibrahim, M. I., Sulaiman, S., Watanabe, I. (September, 2018). *Ab-initio* modeling of the implanted muon in  $\text{YBa}_2\text{Cu}_3\text{O}_6$ . *Poster presentation at 2018 Autumn Meeting, The Physical Society of Japan*. Kyotanabe, Japan.
8. Rozak, H., Zaharim, W.N., Abu Bakar, S.N., Ismail, N.E., Miyazaki, I., Ichimura, K,

## Usage Report for Fiscal Year 2018

- Mohamed-Ibrahim, M. I., Sulaiman, S., Watanabe, I. (September, 2018).  $\mu$ SR Studies on Electron Motion along DNA Molecule. *Poster presentation at 2018 Autumn Meeting, The Physical Society of Japan*. Kyotanabe, Japan.
9. M. R. Ramadhan, I. Ramli, M. D. Umar, S. Winarsih, B. Adiperdana, B. Kurniawan, M. I. Mohamed-Ibrahim, S. Sulaiman, T. Adachi, I. Watanabe. (August, 2018). Muon's Perturbation on the Local Spatial Distribution of Cu-Spin in  $\text{La}_2\text{CuO}_4$  Simulated by Density Functional Theory Calculations. *Poster presentation at the 12<sup>th</sup> International Conference on Materials and Mechanisms of Superconductivity and High Temperature Superconductors*. Beijing, China.
  10. Ramli, I., Mohd-Tajudin, S.S., Ramadhan M.R., Mohamed-Ibrahim, M. I., Sulaiman, S., Nishizaki, T., Kurniawan, B., Watanabe, I. (August, 2018). Density Functional Theory Simulation of Spin Distribution Perturbed by Muon in  $\text{YBa}_2\text{Cu}_3\text{O}_6$ . *Poster presentation at the 12th International Conference on Materials and Mechanisms of Superconductivity and High Temperature Superconductors*. Beijing, China.
  11. Ramli, I., Mohd-Tajudin S.S., Mohamed-Ibrahim, M. I., Sulaiman, S., Watanabe, I. (March, 2018). Implanted Muons in Strongly Correlated System. *Poster presentation at 73rd Annual Meeting 2018, The Physical Society of Japan*. Tokyo, Japan.

### [Others (Book, Press release, etc.)]

1. Superconducting Gap Symmetry in Organic Superconductor  $\lambda$ -(BETS) $_2$ GaCl $_4$  studied by  $\mu$ SR and DFT, D. P. Sari, H. Aizawa, T. Koretsune, and H. Seo. *RIKEN Accel. Prog. Rep. Peer Reviewed*, 51, 206, 2018.
2. M. R. Ramadhan, M. I. Mohamed-Ibrahim, S. Sulaiman, and I. Watanabe. (2018). Effect of Supercell Calculation on Muon Sites in  $\text{La}_2\text{CuO}_4$ . *RIKEN Accel. Prog. Rep. Peer Reviewed*, 51, 197.
3. I. Ramli, S. S. Mohd-Tajudin, S. Sulaiman, M. I. Mohamed-Ismail, and I. Watanabe. (2018). Study of Implanted Muons in  $\text{YBa}_2\text{Cu}_3\text{O}_6$ . *RIKEN Accel. Prog. Rep. Peer Reviewed*, 51, 199.
4. H. Rozak, W. Zaharim, F. Astuti, R. Asih, R. Samian, S. Samsudin, S. N. Abu Bakar, N. Ismail, I. Watanabe, M. I. Mohamed-Ibrahim, S. Sulaiman. (2018). Electron Transport Studies in Biological Molecules with respect to Ageing Science. *RIKEN Accel. Prog. Rep. Peer Reviewed*, 51, 208.